Received: 27 June 2017 | Revised: 10 August 2017 | Accepted: 11 August 2017

DOI: 10.1002/aoc.4098

FULL PAPER

WILEY Applied Organometallic Chemistry

Co(II), Ni(II), Cu(II) and Zn(II) complexes of aminothiazole-derived Schiff base ligands: Synthesis, characterization, antibacterial and cytotoxicity evaluation, bovine serum albumin binding and density functional theory studies

A. Prakash | R. Malhotra

Guru Jambheshwar University of Science and Technology Hissar, 125001, Haryana, India

Correspondence
R. Malhotra, Guru Jambheshwar University of Science and Technology Hissar, 125001, Haryana, India.
Email: malhotra_ksrk@yahoo.co.in

Funding information
Council of Science and Industrial Research, Grant/Award Number: 09/752/(0045)/2012-EMR-1

Transition metal complexes of type $M(L)_2(H_2O)_x$ were synthesized, where L is deprotonated Schiff base 2,4-dihalo-6-(substituted thiazol-2-ylimino)methylphenol derived from the condensation of aminothiazole or its derivatives with 2-hydroxy-3-halobenzaldehyde and M = Co^{2+}, Ni^{2+}, Cu^{2+} and Zn^{2+} ($x = 0$ for Cu^{2+} and Zn^{2+}; $x = 2$ for Co^{2+} and Ni^{2+}). The synthesized Schiff bases and their metal complexes were thoroughly characterized using infrared, ^1H NMR, electronic and electron paramagnetic resonance spectroscopies, elemental analysis, molar conductance and magnetic susceptibility measurements, thermogravimetric analysis and scanning electron microscopy. The results reveal that the bidentate ligands form complexes having octahedral geometry around Co^{2+} and Ni^{2+} metal ions while the geometry around Cu^{2+} and Zn^{2+} metal ions is four-coordinated. The geometries of newly synthesized Schiff bases and their metal complexes were fully optimized in Gaussian 09 using 6–31 + g(d,p) basis set. Fluorescence quenching data reveal that Zn(II) and Cu(II) complexes bind more strongly to bovine serum albumin in comparison to Co(II) and Ni(II) complexes. The ligands and their complexes were evaluated for *in vitro* antibacterial activity against *Escherichia coli* ATCC 25922 (Gram negative) and *Staphylococcus aureus* ATCC 29213 (Gram positive) and cytotoxicity against lever hepatocellular cell line HepG2.

KEYWORDS
antibacterial activity, BSA binding, Co(II), Ni(II), Cu(II) and Zn(II) complexes, cytotoxicity evaluation, DFT studies, Schiff base, spectroscopic studies

1 | INTRODUCTION

Schiff bases are compounds synthesized in high yields by conventional or microwave condensation between equivalent amounts of primary amines and aldehyde or ketones.[1–3] Aminothiazoles, which act as oestrogen receptors and a novel class of adenosine receptor antagonists, when condensed with carbonyl compounds form Schiff base ligands, existing in keto and enolic form, which are of particular interest due to their wide range of applications as antimicrobial,[4] anticancer,[5–7] anti-platelet activity[8] and anti-inflammatory[9] agents and for Alzheimer's disease treatment.[10] These Schiff base ligands have strong coordinative ability due to their synthetic flexibility, selectivity and sensitivity towards metal ions. The activity of these complexes of Schiff base ligands

in biological systems depends on the ease of cleavage of bonds between ligands and metal ions.

The biological importance of the thiazole ring is very well known and reported in the literature. Penicillin, the very first known antibiotic, also contains a tetrahydrothiazole in its skeleton. Thiazolamines are key intermediates for synthesizing many pharmaceuticals.[11] A literature survey revealed that compounds with a thiazole ring show enhanced biological activity.[12] Aminothiazoles are known to be ligands of the oestrogen receptor and as a novel class of adenosine receptor antagonists.[13]

It has been reported that many compounds show a marked enhancement in pharmacological and toxicological properties when combined with metal ions.[14–16] In continuation of our research work[17–20] on the study of the chelation effect on biologically active molecules, we herein report some new Schiff base ligands derived from the condensation of aminothiazole and salicylaldehyde derivatives and their metal complexes to study their antibacterial and cytotoxic properties.

2 | EXPERIMENTAL

2.1 | Materials and methods

All chemicals used were of AnalaR grade and obtained from Sigma-Aldrich and Fluka. Metal salts were purchased from E. Merck and were used as received.

2.2 | General procedure for synthesis of ligands HL_1–HL_3

Ligand HL_1 was synthesized by refluxing equimolar amounts of 5-methyl-2-aminothiazole (1.14 g, 0.01 mol) and 2-hydroxy-3,5-dichlorobenzaldehyde (1.91 g, 0.01 mol) in 50 ml of methanol for 2 h (Scheme 1). The progress of the reaction was monitored by TLC and, after completion of the reaction, the solution was left overnight at room temperature. The solid product separated out, which was filtered, washed and recrystallized from ethanol. The same procedure was used for the synthesis of ligands HL_2 and HL_3.

The structures of the synthesized Schiff bases were characterized using infrared (IR), ^{1}H NMR and mass spectrometry and analytical data.

2.2.1 | 2,4-Dichloro-6-(((5-methylthiazol-2-yl)imino)methyl)phenol (HL_1)

Yield: 78%; colour: yellow; m.p. 152 °C. IR (KBr, cm^{-1}): 1660 ν(HC=N), 3068 ν(—OH). ^{1}H NMR (400 MHz; $CDCl_3$; δ, ppm): 2.50 (s, 5–CH3), 7.34 (d, 6′–H), 7.36 (s, 4–H), 7.48 (d, 4′–H), 9.08 (s, N=CH), 13.04 (s, −OH). MS (ESI): $[M + H]^+ = 287.88$.

2.2.2 | 2-Bromo-4-chloro-6-(((5-methylthiazol-2-yl)imino)methyl)phenol (HL_2)

Yield: 83%; colour: orange; m.p. 136 °C. IR (KBr, cm^{-1}): 1672 ν(HC=N), 3080 ν(—OH). ^{1}H NMR (400 MHz;

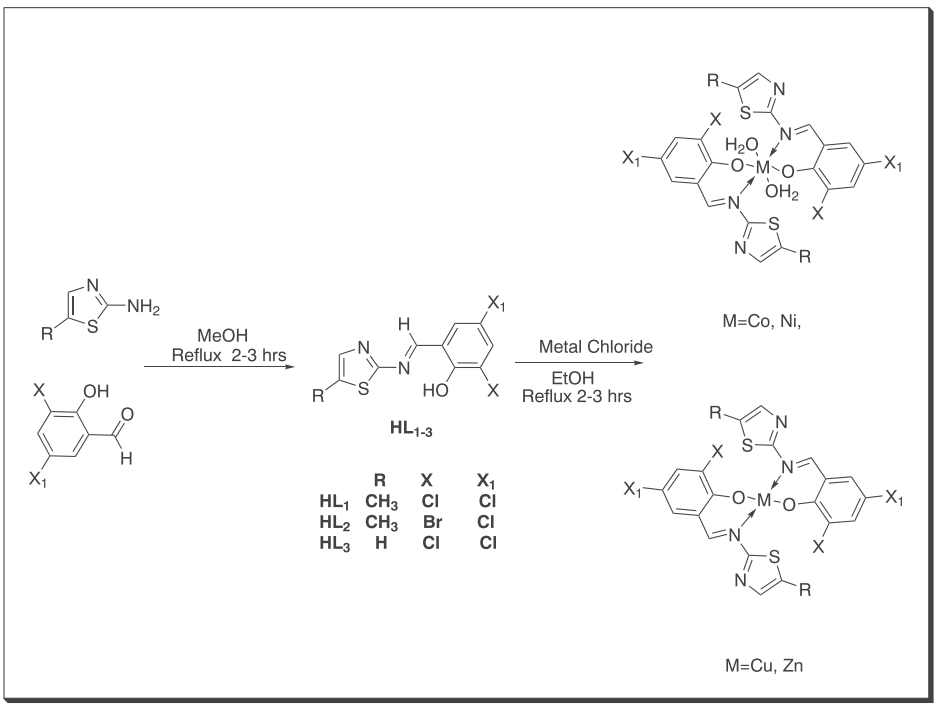

SCHEME 1 Synthesis of Schiff base ligands and metal complexes

$CDCl_3$; δ, ppm): 2.49 (s, 5–CH3), 7.35 (s, 4–H), 7.37 (d, 6′–H), 7.63 (d, 4′–H), 9.05 (s, N=CH), 13.18 (s, −OH). MS (ESI): $[M + H]^+ = 330.71$.

2.2.3 | 2,4-Dichloro-6-((thiazol-2-ylimino) methyl)phenol (HL_3)

Yield: 69%; colour: pale yellow; m.p. 168 °C. IR (KBr, cm^{-1}): 1653 ν(HC=N), 3051 ν(—OH). ^1H NMR (400 MHz; $CDCl_3$; δ, ppm): 7.34 (d, 4–H), 7.37 (d, 6′–H), 7.50 (d, 4′–H), 7.70 (d, 5–H) 9.18 (s, N=CH), 13.02 (s, −OH). MS (ESI): $[M + H]^+ = 272.92$.

2.3 | General procedure for synthesis of metal complexes 1–12

The metal complexes (**1**–**4**) of ligand HL_1 were prepared by mixing a hot ethanolic solution (20 ml) of HL_1 (0.56 g, 2 mmol) with an ethanolic solution (20 ml) of salt of Co(II) (0.238 g, 1 mmol), Ni(II) (0.238 g, 1 mmol), Cu(II) (0.170 g, 1 mmol) or Zn(II) (0.136 g, 1 mmol). The reaction mixture was stirred for 1 h followed by refluxing for 4–18 h. The solvent was reduced to half and the reaction mixture was kept overnight. The product separated out, which was filtered off, washed with cold ethanol and ether and dried under vacuum over P_4O_{10}.

The Co(II), Ni(II), Cu(II) and Zn(II) complexes (**5**–**12**) of ligands HL_2 and HL_3 were prepared using a similar procedure. Physical, analytical and spectral data of ligands and metal complexes are given in Table 1.

2.4 | Analysis

^1H NMR spectra were recorded with a Bruker 400 MHz NMR spectrometer and the chemical shifts were reported in ppm relative to tetramethylsilane as an internal

TABLE 1 Physical measurements and analytical data of ligands (HL_1–HL_3) and metal complexes(**1**–**12**)

Compound	Molecular mass/ molecular formula	*m/z*	Yield (%)	Melting point (°C)	Elemental analysis: found (calcd)			
					C (%)	H (%)	N (%)	M (%)[a]
HL_1	$C_{11}H_8Cl_2N_2OS$	287.18	78	152	46.13 (46.01)	2.84 (2.81)	9.62 (9.76)	—
HL_2	$C_{11}H_8BrClN_2OS$	330.71	83	136	39.86 (39.84)	2.39 (2.43)	8.45 (8.52)	—
HL_3	$C_{10}H_6Cl_2N_2OS$	272.92	69	168	43.83 (43.97)	2.20 (2.21)	10.32 (10.26)	—
1	$Co(L_1)_2(H_2O)_2$ $C_{22}H_{18}Cl_4CoN_4O_4S_2$	665.64	62	>260	39.42 (39.60)	2.59 (2.72)	8.43 (8.40)	9.12 (8.83)
2	$Ni(L_1)_2(H_2O)_2$ $C_{22}H_{18}Cl_4N_4NiO_4S_2$	664.02	58	>260	39.53 (39.61)	2.70 (2.72)	8.49 (8.40)	9.02 (8.80)
3	$Cu(L_1)_2$ $C_{22}H_{14}Cl_4CuN_4O_2S_2$	633.92	67	>260	41.68 (41.56)	2.26 (2.22)	8.78 (8.81)	9.91 (9.99)
4	$Zn(L_1)_2$ $C_{22}H_{14}Cl_4N_4O_2S_2Zn$	634.64	65	>260	41.36 (41.44)	2.17 (2.21)	8.78 (8.79)	10.41 (10.25)
5	$Co(L_2)_2(H_2O)_2$ $C_{22}H_{18}Br_2Cl_2CoN_4O_4S_2$	753.21	56	>260	35.14 (34.94)	2.47 (2.40)	7.58 (7.41)	7.68 (7.79)
6	$Ni(L_2)_2(H_2O)_2$ $C_{22}H_{18}Br_2Cl_2N_4NiO_4S_2$	752.84	57	>260	34.86 (34.95)	2.44 (2.40)	7.60 (7.41)	7.91 (7.76)
7	$Cu(L_2)_2$ $C_{22}H_{14}Br_2Cl_2CuN_4O_2S_2$	721.72	75	>260	37.05 (36.46)	2.08 (1.95)	7.61 (7.73)	8.84 (8.77)
8	$Zn(L_2)_2$ $C_{22}H_{14}Br_2Cl_2N_4O_2S_2Zn$	722.29	79	>260	36.43 (36.37)	1.98 (1.94)	7.64 (7.71)	9.07 (9.00)
9	$Co(L_3)_2(H_2O)_2$ $C_{20}H_{14}Cl_4CoN_4O_4S_2$	637.11	82	>260	37.81 (37.58)	2.27 (2.21)	8.76 (8.76)	9.36 (9.22)
10	$Ni(L_3)_2(H_2O)_2$ $C_{20}H_{14}Cl_4N_4NiO_4S_2$	637.01	72	>260	37.60 (37.59)	2.34 (2.21)	8.92 (8.77)	9.14 (9.19)
11	$Cu(L_3)_2$ $C_{20}H_{10}Cl_4CuN_4O_2S_2$	605.32	67	>260	39.46 (39.52)	1.69 (1.66)	9.37 (9.22)	10.67 (10.45)
12	$Zn(L_3)_2$ $C_{20}H_{10}Cl_4N_4O_2S_2Zn$	606.12	63	>260	39.47 (39.40)	1.68 (1.65)	9.16 (9.19)	10.86 (10.72)

[a]M = Co(II), Ni(II), Cu(II), Zn(II).

standard. IR spectra were recorded with a Shimadzu IR affinity-I 8000 FT-IR spectrometer using KBr discs. Electrospray ionization (ESI) mass spectra were obtained using a VG Biotech Quattrro mass spectrometer equipped with an ESI source in the mass range m/z 100 to 1000. UV spectra were recorded in dimethylsulfoxide (DMSO) with a Varian Cary-5000 spectrometer. Electron paramagnetic resonance (EPR) spectra of the Cu(II) complexes were recorded using a JES FA200 ESR X-band spectrometer using tetracyanoethylene as the internal reference. Elemental analysis was carried out with a PerkinElmer 2400. Thermogravimetric analysis (TGA) of samples was carried out using an SDT-Q600 simultaneous TGA/DSC instrument at a heating rate of 10 °C min^{-1}. Magnetic moments at room temperature of the complexes were calculated by Gouy's method, using Hg[Co(SCN)4] as the calibrant. Molar conductance measurements of 10^{-3} M solutions of metal complexes in dimethylformamide (DMF) were conducted using a Systronics model 306 conductivity bridge.

2.5 | Antibacterial activity

Escherichia coli ATCC 25922 (Gram negative) and *Staphylococcus aureus* ATCC 29213 (Gram positive) were cultured according to ATCC recommendations (American Type Culture Collection, Manassas, USA). Colonies were isolated from freshly streaked Mueller–Hinton agar plate. A bacterial inoculum of 5×10^5 CFU ml^{-1} was prepared after adjusting to McFarland's standard following CLSI guidelines. Ampicillin was used as reference drug and DMSO as a negative control. Stocks for test compounds and ampicillin were appropriately diluted (total 11 dilutions in duplicate) to achieve a final concentration range of 64 to 0.0625 μg ml^{-1} with 100% DMSO. Diluted compounds were added into cation-adjusted Mueller–Hinton Broth (CAMHB) and bacterial suspension was finally added to it. Plates were placed in a 37 °C air incubator and incubated for 18–20 h followed by turbidity measurement at 600 nm (Spectra Max M5, Molecular Devices). Minimum inhibitory concentration (MIC) was interpreted as the lowest concentration of antimicrobial agent that completely inhibited growth of an organism.

2.6 | Cytotoxicity assessment

Effects of compounds on the viability of human cancer (hepatocellular) cell lines were determined by colorimetric assay using 3-(4,5-dimethylthiazol-2-yl)-2,5-diphenyltetrazolium bromide (MTT). HepG2 cells were procured from ATCC and cultured according to ATCC instructions. Around 8500 cells per well were plated in a 96-well plate 24 h prior to the experiment and incubated at 37 °C in a CO_2 incubator. Cells were treated with either vehicle (1% DMSO) or serially diluted test compounds (30 μg ml^{-1}) or doxorubicin (10 μM as positive control) or 0.1% Triton (reference control) in a final volume of 200 μl per well and incubated at 37 °C in a CO_2 incubator for 72 h. Following incubation, cells were treated with 100 μg of MTT and incubated at 37 °C for 4 h. Supernatants were removed carefully (without disturbing the formazan crystals formed) and 70 μl of DMSO was added to each well. The plate was kept on a plate shaker until the crystals were dissolved and the absorbance was read at 540 nm. The absorbance values from test compound wells were compared to that for the control wells to calculate the percentage inhibition. Inhibition was calculated with respect to 0.1% Triton (100% inhibition) and 1% DMSO (0% inhibition).

2.7 | Protein binding studies

Fluorescence study of metal complex binding with bovine serum albumin (BSA) was performed using a spectrofluorimeter (FS920, Edinburgh Instruments, UK) with standard 3.5 ml quartz cell. The excitation source was a xenon lamp (450 W) and the sample chamber was equipped with a Peltier accessory. Scanning parameters for all measurements were optimized with slit width of 4.0 nm for excitation and emission, dwell time of 0.2 s and wavelength step of 1 nm. The emission spectra were recorded in the wavelength range 310–450 nm at a scan rate of 100 nm min^{-1}.

2.8 | Density functional theory (DFT) calculations

DFT calculations were performed with the Gaussian 09 W program using the 6–31 + g(d,p) basis set.[21] The geometries with respect to energy were fully optimized using the B3LYP three-parameter density functional, which includes Becke's gradient exchange correction,[22] the Lee, Yang, Parr correlation functional[23] and the Vosko, Wilk, Nusair correlation functional.[24]

3 | RESULTS AND DISCUSSION

Schiff bases (HL_1–HL_3) are obtained by the nucleophilic addition of the —NH_2 group of 2-aminothiazoles to the carbonyl group of substituted aromatic hydroxyaldehydes as shown in Scheme 1.

The crystalline solids so obtained have different shades of yellow or orange colour due to the presence of chromophoric group (HC=N) in the molecule. All the metal complexes were prepared by direct reaction

between Schiff base and corresponding metal salt. The synthesized complexes are crystalline solids and stable in air at room temperature. The melting points of the metal complexes are much higher than those of the ligands, which indicates that these complexes are much more stable as compared to the ligands. The complexes in 10^{-3} M DMF solution have low molar conductance values (8.5–12.8 Ω^{-1} cm^2 mol^{-1}) indicating their non-electrolyte nature.[25]

3.1 | ^{1}H NMR spectra

The ^{1}H NMR spectra of the ligands and their Zn(II) complexes were recorded in $CDCl_3$ containing a small amount of DMSO-d_6 with tetramethylsilane as internal reference to confirm the structure of the ligands and the mode of bonding in Zn(II) complexes. The presence of azomethine proton of all the aldimines was confirmed by observing one proton singlet at 9.03–9.18 ppm. Two doublets corresponding to one proton each assigned to CH=CH of thiazolyl group was observed at 7.5 ppm in the case of HL_3. One proton singlet assigned to phenolic proton was observed at 13.02–13.18 ppm for all the ligands. Signals due to aromatic protons were observed at 7.3–7.7 ppm. A comparison of ^{1}H NMR spectra of the ligands and their Zn(II) complexes gives a clue to the mode of binding of ligand to zinc metal. The one-proton singlet in the range 13.02–13.18 ppm in the spectra of HL_1–HL_3, which corresponds to —OH proton, completely disappeared after complex formation. The disappearance of the singlet due to OH group of the free ligand indicates the deprotonation of —OH proton during metal complexation. A slight downfield shift (9.27 ppm) was observed for azomethine proton as compared to the ligands suggesting the coordination of azomethine nitrogen to Zn(II) ion, while the rest of the signals due to aromatic and thiazolyl protons remain almost unaltered. A comparison of the ^{1}H NMR spectra of HL_3 and $Zn(L_3)_2$ complex is shown in Figure 1.

3.2 | Mass spectra

In the ESI mass spectrum of ligand HL_1, a peak corresponding to $[M + H]^+$ ion appears as molecular ion peak at m/z = 287.88 amu. The molecular ion peak confirms the proposed formula ($C_{11}H_8Cl_2N_2OS$). Peaks corresponding to various fragments of HL_1 appear at 287.18, 203.98, 180.81, 179.68, 177.95, 101.98 and 73.99 amu. Similarly, for ligands HL_2 and HL_3, the molecular ion peak appears at 330.71 and 272.92 amu, respectively. The m/z values for metal complexes **1**–**12** are given in Table 1.

3.3 | IR spectra

To understand the binding mode of the ligands to the corresponding metal ions, IR spectral data of HL_1–HL_3 and their metal complexes are compared. The coordination of the ligand to the corresponding metal ion was confirmed on the basis of shifts in absorption bands of various groups and absence of certain absorptions (Table 2). In the IR spectra of the ligands, the bands originally attributed to ν(C=O) of aldehyde and $\nu(NH_2)$ of aminothiazole

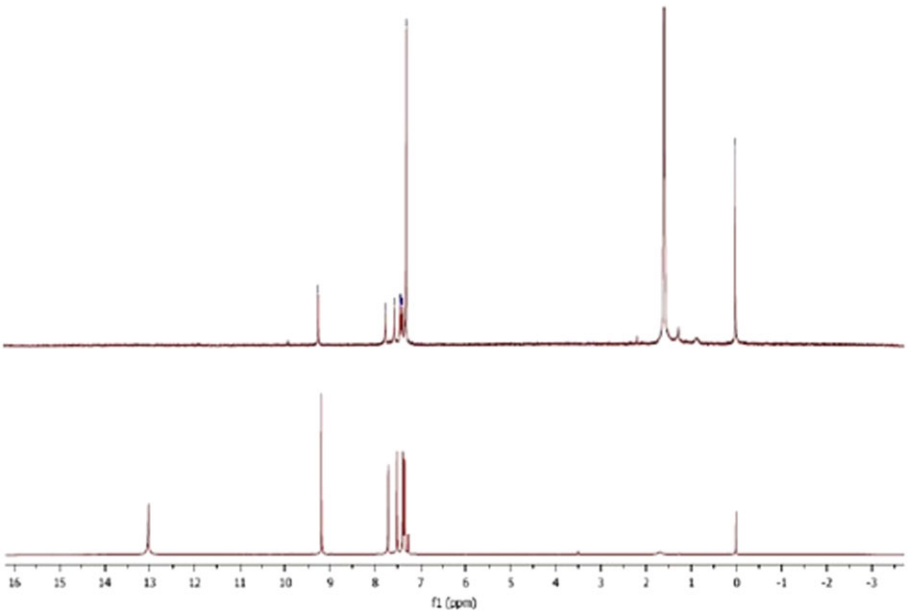

FIGURE 1 Comparison of ^{1}H NMR spectra of HL_3 and $Zn(L_3)_2$

TABLE 2 Important IR spectral bands (cm^{-1}) and assignments

Compound	ν(C=N)	ν(OH)	ν(M—O)	ν(M—N)
HL_1	1660	3068	—	—
1	1638	—	555	418
2	1639	—	567	422
3	1641	—	562	424
4	1642	—	551	436
HL_2	1672	3080	—	—
5	1657	—	542	427
6	1651	—	547	439
7	1653	—	561	459
8	1654	—	549	449
HL_3	1653	3051	—	—
9	1639	—	534	416
10	1633	—	567	432
11	1631	—	563	428
12	1633	—	557	441

at 1750, 3320 and 3460 cm^{-1}, respectively, of the starting materials were absent. Instead, a new band appeared at 1653–1672 cm^{-1}, assigned to ν(HC=N) vibration, which confirms the formation of Schiff base.[26] Comparison of the IR spectral data of the ligands and the metal complexes reveals that the band corresponding to ν(HC=N) vibration shifts in frequency by 20–25 cm^{-1} for all the metal complexes, which indicates the involvement of nitrogen of azomethine in metal complexation.[27] This is further supported by the appearance of a new band at 416–459 cm^{-1} due to ν(M—N) stretching vibrations.[28] A band at 3051–3080 cm^{-1} in the IR spectra of ligands is due to ν(—OH) stretching vibration and the low value may be due to hydrogen bonding between OH and nitrogen of azomethine. The absence of this band in the IR spectra of metal complexes indicates the deprotonation of phenolic OH on metal complexation and coordination through phenolic oxygen. This was further confirmed by the appearance of a weak low-frequency band at 534–567 cm^{-1} due to ν(M—O).[29] The presence of coordinated water molecule in complexes of Co^{2+} and Ni^{2+} metal ions was confirmed by the presence of a broad band observed in the range 3273–3454 cm^{-1},[30] while no such band was observed in the spectra of the Cu^{2+} and Zn^{2+} complexes.

TABLE 3 EPR data for Cu(II) complexes

Complex	$g_{\|\|}$	$g_{\perp}$	g_{av}	G	λ	α^2
$Cu(L_1)_2$	2.22	2.08	2.13	2.80	−501	0.62
$Cu(L_2)_2$	2.24	2.08	2.13	3.05	−509	0.69
$Cu(L_3)_2$	2.23	2.09	2.14	2.60	−534	0.66

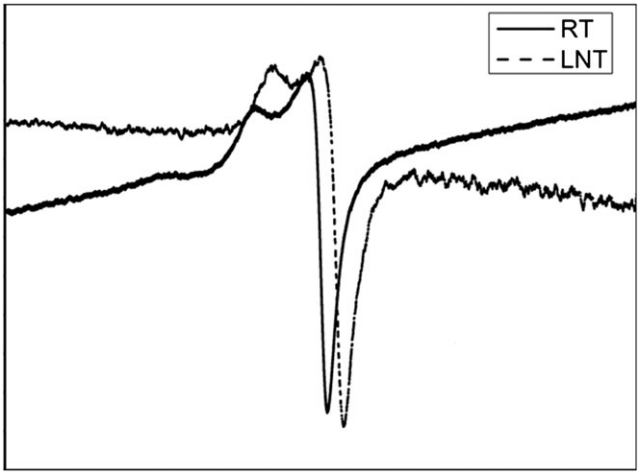

FIGURE 2 EPR spectra of $Cu(L_2)_2$ (RT, room temperature; LNT, liquid nitrogen temperature)

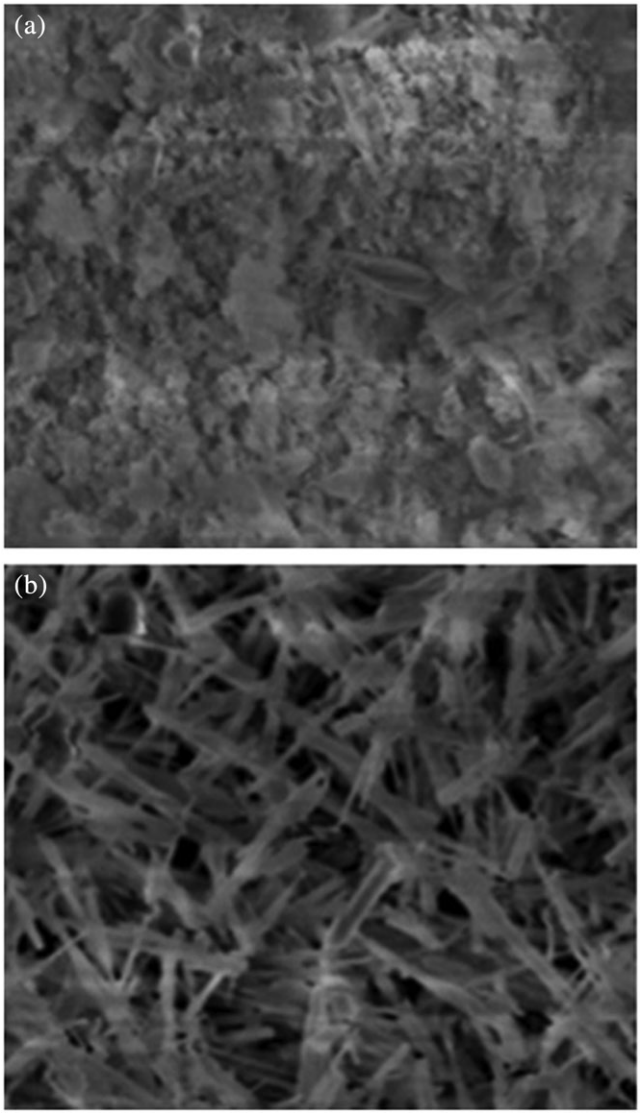

FIGURE 3 Scanning electron microscopy images of (a) HL_3 and (b) $Cu(L_3)_2$

3.4 | Conductance and magnetic susceptibility measurements

The molar conductance values of metal complexes **1–12** were obtained in DMF as a solvent at room temperature. The molar conductance of the metal complexes in DMF showed values (8.5–12.8 Ω^{-1} cm^2 mol^{-1}) indicating that complexes **1–12** are non-electrolytes.[25]

The magnetic moment values of all the metal complexes at room temperature were recorded. The magnetic moment values of Co(II) complexes were found to be in the range 4.94–5.02 BM, suggesting the Co(II) complexes in an octahedral environment.[29] Ni(II) complexes have magnetic moment values in range 2.93–2.97 BM corresponding to two unpaired electrons, indicating a triplet ground state having octahedral geometry around the metal ion.[29] Cu(II) complexes show magnetic moment values of 1.69–1.74 BM, which indicate a square planar arrangement around the Cu(II) ion.

3.5 | Electronic spectra

The electronic spectra of Co(II) complexes derived from ligands HL_1 and HL_2 show two bands in the region 15 200–16 900 and 21 000–22 000 cm^{-1} assigned to $^4T_{1g}(F) \rightarrow {}^4A_{2g}(F)$ (ν_2) and $^4T_{1g}(F) \rightarrow {}^4T_{1g}(P)$ (ν_3) transitions, respectively, while the complex obtained from ligand HL_3 gives three bands in the region 9700–10 000 (ν_1), 15 000–16 000 (ν_2) and 22 400–23 100 cm^{-1} (ν_3) which are in accordance with octahedral geometry around the Co^{2+} ion.[27] The high-energy band at 29 000–30 000 cm^{-1} for all the complexes is assigned to metal–ligand charge transfer band. The Ni(II) complexes show three bands in the regions 10 300–10 700, 16 200–17 200 and 24 700–25 300 cm^{-1} assigned to $^3A_{2g}(F) \rightarrow {}^3T_{2g}(F)$, $^3A_{2g}(F) \rightarrow {}^3T_{1g}(F)$ and $^3A_{2g}(F) \rightarrow {}^3T_{1g}(P)$, respectively, indicating octahedral geometry around Ni^{2+} complexes.[31]

The electronic spectra of Cu(II) complexes show two low-energy weak bands assigned to $^2B_{1g} \rightarrow {}^2A_{1g}$ and $^2B_{1g} \rightarrow {}^2E_g$ transitions at 15 250–15 670 and 20 000–20 500 cm^{-1}, respectively.[31] A strong high-energy band at 30 100–30 900 cm^{-1} is assigned to metal–ligand charge transfer.

3.6 | EPR spectra

The solid-state X-band EPR spectra of Cu(II) polycrystalline solid complexes were recorded in powder form at room temperature and in DMSO at 77 K. The EPR spectrum of $Cu(L_1)_2$ at room temperature displayed an isotropic signal having axially symmetric line shape with two g values, i.e. $g_{||} = 2.22$ and $g_{\perp} = 2.08$, and g_{av} was computed

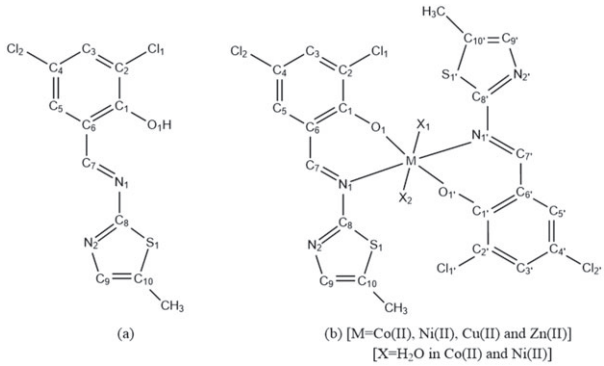

FIGURE 4 Numbering schemes of (a) ligand HL_1 and (b) metal complexes **1–4**

TABLE 4 Thermal analysis data for metal complexes **1–4**

Complex	Molecular formula	Stage	Temp. (°C)	Possible evolved species	Residual species	Mass loss (%) Found	Mass loss (%) Calcd
1	$Co(L_1)_2(H_2O)_2$	1	120–160	$2H_2O$	CoO	5.43	5.41
	$C_{22}H_{18}Cl_4CoN_4O_4S_2$	2	160–390	$C_8H_{10}N_2S_2$		29.72	29.67
		3	390–800	Remaining moiety		53.51	53.68
						11.34	11.24
2	$Ni(L_1)_2(H_2O)_2$	1	140–190	$2H_2O$	NiO	5.51	5.26
	$C_{22}H_{18}Cl_4N_4NiO_4S_2$	2	190–410	C_5H_5NS		15.11	14.90
		3	370–800	Remaining moiety		67.93	68.7
						11.45	11.14
3	$Cu(L_1)_2$	1	110–380	$C_{10}H_{10}N_2S_2Cl_4$	CuO	56.89	57.18
	$C_{22}H_{14}Cl_4CuN_4O_2S_2$	2	380–800	Remaining moiety		30.22	30.44
						12.87	12.48
4	$Zn(L_1)_2$	1	120–360	$C_{10}H_{10}N_2S_2$	ZnO	34.94	35.01
	$C_{22}H_{14}Cl_4N_4O_2S_2Zn$	2	390–670	Organic moiety		52.14	52.38
						12.92	12.61

using the relation $g_{av} = 1/3(g_{||} + 2g_{\perp})$. From the observed values it is clear that $g_{||} > g_{\perp} > 2.0023$, and these parameters are well consistent with related systems which suggest a square planer geometry around Cu(II) metal ion, with an unpaired electron lying predominantly in the $d_{x^2-y^2}$ orbital giving $^2B_{1g}$ as the ground state. The value of $g_{||}$ also helps in predicting the ionic and covalent environment in metal–ligand bonding. The $g_{||}$ values being less than 2.3 is an indication of significant covalent bonding in Cu(II) complexes.[32] The value of exchange interaction term G calculated using $G = (g_{||} - 2.0023)/(g_{\perp} - 2.0023)$ gives an idea about exchange interactions between Cu(II) centres. The value of $G < 4.0$ indicates negligible exchange interactions of Cu–Cu in the complex. The spin–orbital coupling constant λ values (−534 to −501 cm^{-1}) calculated using the relation $g_{av} = 2(1–2\lambda/10Dq)$ are less than that for the free Cu^{2+} ion (−828 cm^{-1}) which supports the covalent character of metal–ligand bond in these complexes. The fraction of unpaired electron density located on Cu^{2+} ion, i.e. the value of in-plane σ-bonding parameter α^2 was calculated using the expression $\alpha^2 = -(A_{||}/0.036) + (g_{||} - 2.0023) + 3/7(g_{\perp} - 2.0023) + 0.04$ (Table 3). From the value of α^2, we can predict the ionic or covalent character in metal complexes: a value of α^2 of 0.5 indicates covalent bonding, while a value of 1.0 suggests complete ionic bonding. The calculated values of α^2 (0.62–0.69) of the Cu(II) complexes indicate that these are fairly covalent. The EPR spectra of $Cu(L_2)_2$ complex is displayed in Figure 2.

3.7 | Scanning electron microscopy

On comparison of the scanning electron microscopy images of free ligand (HL_3) and metal complex ($[Cu(L_3)_2]$) (Figure 3), it is clear that a crystalline image of the complex was obtained after the complexation process. These complexes have agglomerated morphological structures. Cu(II) complexes have needle-like structure while the other complexes have broken stone-like structure. Efforts made to isolate single crystal of these complexes were not successful. So to understand better the electronic and molecular structures of the synthesized ligands and metal complexes, DFT calculation was performed.

3.8 | Thermogravimetric analysis

Thermal behaviour of complexes was investigated using the TGA technique. TGA of metal complexes **1**–**4** was carried out with temperature ranging from room temperature to 800 °C. The TGA curves show that metal complexes **1**–**4** decompose in three steps. The first step in the TGA curve (110–260 °C) of $Ni(H_2O)_2(L_1)_2$/$Co(H_2O)_2(L_1)_2$ corresponds

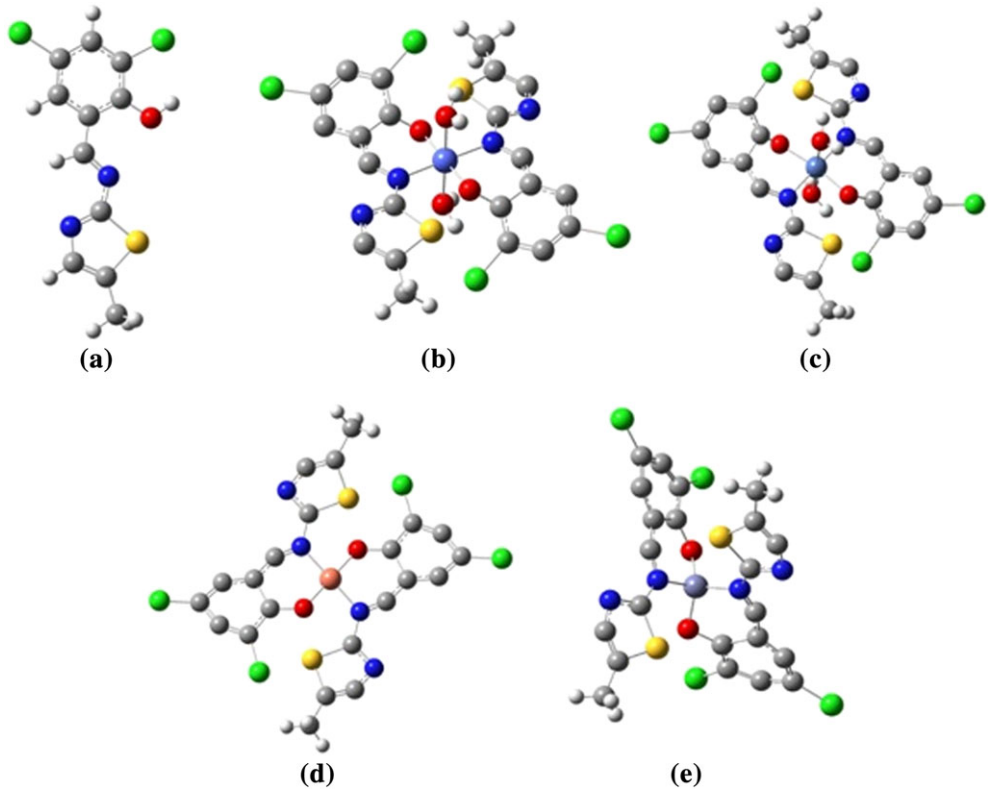

FIGURE 5 Optimized structures of (a) ligand HL_1, (b) $[Co(L_1)_2(H_2O)_2]$, (c) $[Ni(L_1)_2(H_2O)_2]$, (d) $[Cu(L_1)_2]$ and (e) $[Zn(L_1)_2]$

to the loss of coordinated water molecules in the complex, while no such loss of weight is observed in the case of $Zn(L_1)_2/Cu(L_1)_2$ complex in the same temperature range, eliminating the possibility of coordinated water present in the complex. The second and third steps correspond to the loss of organic moiety leaving metal oxide as the final residue. Based on the thermograms, decomposition stages, temperature ranges, decomposition product as well as weight loss percentages of the complexes were calculated (Table 4).

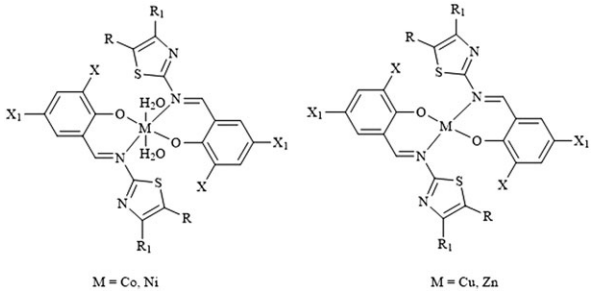

FIGURE 6 Proposed structures of metal complexes

TABLE 5 Optimized geometry of ligand HL_1 and metal complexes **1**–**4** (bond lengths in angstroms; bond angles in degrees)

Parameter[a]	Ligand HL_1	Complex 1	Complex 2	Complex 3	Complex 4
C_1–O_1	1.370	1.563	1.561	1.545	1.536
C_1–C_2	1.403	1.437	1.456	1.491	1.458
C_2–C_3	1.390	1.398	1.392	1.391	1.403
C_3–C_4	1.394	1.401	1.410	1.427	1.415
C_4–C_5	1.386	1.389	1.398	1.401	1.393
C_5–C_6	1.413	1.409	1.411	1.436	1.428
C_1–C_6	1.432	1.491	1.524	1.591	1.528
C_6–C_7	1.459	1.478	1.491	1.501	1.494
C_7–N_1	1.334	1.293	1.320	1.318	1321
N_1–C_8	1.427	1.487	1.501	1.543	1.508
C_8–N_2	1.376	1.381	1.383	1.395	1.381
N_2–C_9	1.385	1.396	1.402	1.409	1.404
C_9–C_{10}	1.390	1.401	1.407	1.401	1.405
C_{10}–S_1	1.832	1.813	1.875	1.892	1.888
C_8–S_1	1.839	1.890	1.934	1.949	1.921
M–O_1	—	2.109	2.007	2.190	2.098
M–O_1,	—	2.116	2.019	2.212	2.124
M–N_1	—	2.048	2.134	2.378	2.097
M–N_1,	—	2.046	2.098	2.421	2.103
M–X_1	—	2.067	2.012	—	—
M–X_2	—	2.082	2.101	—	—
∠O_1MX_1	—	91.57	83.12	—	—
∠O_1MN_1	—	82.56	79.34	99.12	107.10
∠N_1MX_2	—	86.23	87.72	—	—
∠X_2MO_1,	—	89.23	82.38	—	—
∠O_1,MN_1,	—	82.14	81.23	101.24	108.23
∠N_1,MX_1	—	87.12	78.92	—	—
∠O_1MO_1,	—	173.20	170.12	172.12	101.12
∠X_1MX_2	—	171.27	177.20	—	—
∠N_1MN_1,	—	174.12	170.45	175.34	103.13

[a]See Figure 4 for numbering.

3.9 | Geometry optimization

Ligand HL_1 and metal complexes **1**–**4** were fully optimized in the gas phase with respect to energy using B3LYP functional and 6–31 + g(d,p) basis set in Gaussian 09 W software. The numbering scheme used to compute bond lengths and bond angles for ligand HL_1 and complexes is shown in Figure 4, and the structures of the fully optimized geometries are shown in Figure 5. Ligand HL_1 coordinates through azomethine nitrogen and deprotonated hydroxyl oxygen to Co(II) ion in $(ML_1)_2$ type complex **1** in an octahedral fashion. The other two positions are occupied by water molecules. The optimized structure shows that the geometry around the metal centre is distorted octahedral and the computed bond lengths around the metal centre are slightly elongated when compared with free ligand. This might be possible because of the electron transfer from ligand to metal. The ligand which has a planar structure loses its planarity after metal complexation. The two chlorine atoms move out of the plane in opposite directions. The computed bond lengths for the ligand and the metal complexes are given in Table 5.

After metal coordination, slight deformation was noticed in complex **1** in the ligand moiety. Because of this deformation the bond lengths C_1–O_1, C_1–C_1, C_1–C_6, C_7–N_1 and N_1–C_2 elongate slightly. The bond length C_1–O_1 which was 1.370 Å in free ligand elongates to 1.563, 1.561, 1545 and 1.536 Å, respectively, in metal complexes **1**–**4**. A similar trend was observed for other bond length values. A slight difference in bond length values causes a deviation of bond angle from regular 90° around the metal centre. Bond angles $\angle O_1MX_1$, $\angle O_1MN_1$, $\angle N_1MX_2$, $\angle X_2MO_{1'}$, $\angle O_{1'}MN_{1'}$ and $\angle N_{1'}MX_1$ were found to be 91.57°, 82.56°, 86.23°, 89.23°, 82.14° and 87.12°, respectively. No appreciable change was observed in bond length and bond angle values in benzene and thiazole moiety.

The Ni(II) complex (**2**) also showed distorted octahedral geometry as observed from the computed parameters. Complex **3** which is Cu(II) complex stabilized in square planar geometry and Zn(II) complex which is complex **4**

TABLE 6 Cytotoxicity activity of ligands HL_1–HL_3 and metal complexes **1**–**12**

Compound	Concentration (μg ml^{-1})	Optical density at 540 nm			Inhibition (%)
		n_1	n_2	Average	
HL_1	30	0.4976	0.513	0.505	8
HL_2	30	0.5508	0.5559	0.553	0
HL_3	30	0.2489	0.2635	0.256	59
$Co(L_1)_2(H_2O)_2$	30	0.4255	0.427	0.426	24
$Ni(L_1)_2(H_2O)_2$	30	0.219	0.234	0.227	65
$Cu(L_1)_2$	30	0.5457	0.5387	0.542	1
$Zn(L_1)_2$	30	0.324	0.3286	0.326	45
$Co(L_2)_2(H_2O)_2$	30	0.5221	0.5294	0.525	4
$Ni(L_2)_2(H_2O)_2$	30	0.5068	0.5004	0.504	9
$Cu(L_2)_2$	30	0.6109	0.591	0.601	−11
$Zn(L_2)_2$	30	0.5627	0.5633	0.563	−4
$Co(L_3)_2(H_2O)_2$	30	0.437	0.474	0.456	18
$Ni(L_3)\ (H_2O)_{22}$	30	0.561	0.568	0.565	−4
$Cu(L_3)_2$	30	0.5576	0.5832	0.570	−5
$Zn(L_3)_2$	30	0.5463	0.547	0.547	0
Plate 1	(1%) DMSO control	0.546	0.545	0.545	0
	Doxorubicin(10 μM)	0.110	0.110	0.110	89
	(0.1%) Triton	0.0542	0.0553	0.055	100
Plate 2	(1%) DMSO control	0.556	0.552	0.554	0
	Doxorubicin (10 μM)	0.112	0.109	0.111	89
	(0.1%) Triton	0.0554	0.0552	0.055	100
Plate 3	(1%) DMSO control	0.511	0.523	0.517	0
	Doxorubicin (10 μM)	0.102	0.105	0.104	89
	(0.1%) Triton	0.0541	0.0553	0.055	100

display tetrahedral geometry with a similar trend in computed parameters. The computed bond lengths and bond angles of complexes **1**–**4** are given Table 5.

We also conducted charge analysis for metal complexes **1**–**4** and the results show that, in complex **1**, the electronic configuration of Co(II) is: [core]$4s^{0.02}3d^{6.81}4p^{0.72}5s^{0.18}5p^{0.01}$, plus 18 core electrons, 7.74 valence electrons and 0.026 Rydberg electrons for a total of 25.766 electrons and is in agreement with the calculated natural charge on Co(II) (+01.233*e*). Similar results are found for complexes **2**–**4** and the results are in agreement with the charges found on metal ion. On the basis of these above calculated results, structures can be anticipated for the synthesized metal complexes, as shown in Figure 6.

3.10 | Antibacterial activity

All the compounds were tested against two bacteria: Gram-negative *E.coli* and Gram-positive *S. aureus*. The results were compared with those for the standard drug ampicillin. It has been reported that the nitrogen of azomethine group having a lone pair of electrons has considerable biological importance. The activity of the ligand therefore may be expected to be due to the presence of toxophorically important azomethine and thiazolyl groups, which may involve hydrogen bonding with active centres of specific cell enzymes, thereby resulting in interference with normal cell processes. But the results unexpectedly showed that all the ligands and many of the metal complexes of these ligands exhibit inhibition (MIC > 64 μg ml^{-1}) towards the tested microorganisms under similar experimental conditions. In the case of metal complex $Cu(L_1)_2$ (MIC > 16 μg ml^{-1}) an enhancement was observed in antimicrobial activity of the ligand on coordination to metal ion against *S. aureus* (Gram positive) under similar experimental conditions. This increase in the activity on complexation as compared to free ligand is explained on the basis of chelation theory. The positive charge on metal ion is decreased upon coordination through donor atoms of the ligand and thus reducing the polarity of the metal ion due to which π-electron delocalization occurs within the whole chelate ring system. This process increases the lipophilic nature of the metal atom which favours its penetration through the lipid layer of the membrane wall of the microorganism thus destroying it more effectively.

3.11 | Cytotoxicity bioassay

From the cytotoxicity data it may be concluded that ligands HL_1 and HL_3 obtained by the condensation of

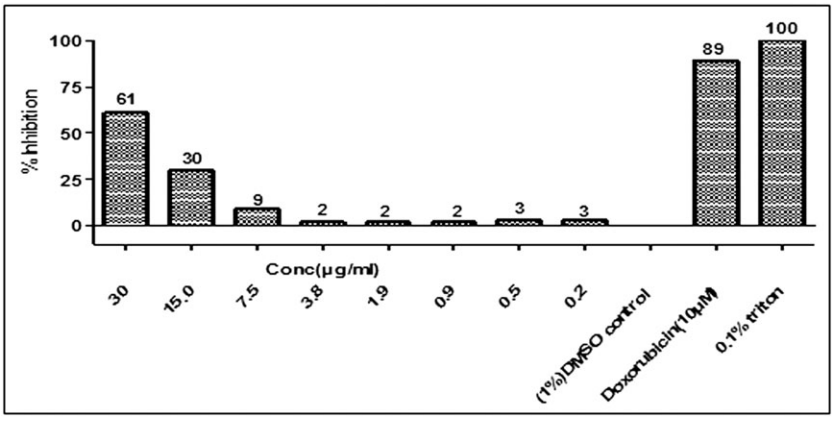

FIGURE 7 Dose–response curve of HL_3

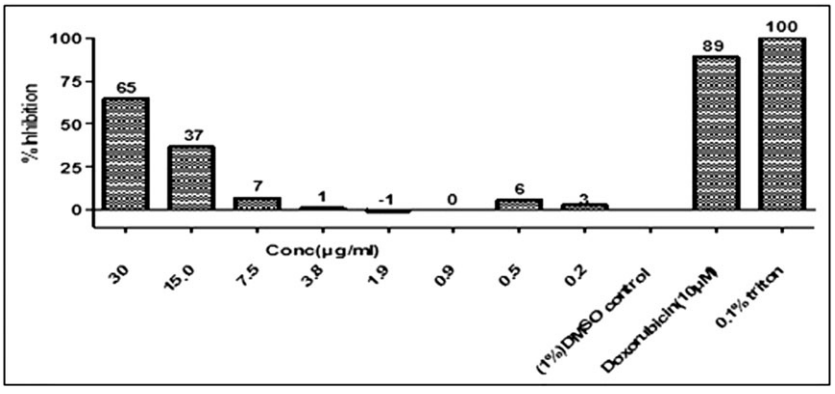

FIGURE 8 Dose–response curve of $Ni(L_3)_2(H_2O)_2$

aminothiazole or methyl-substituted aminothiazole with 3,5-dichlorosalicylaldehyde are active against human cancer cell line HepG2, while ligand HL_2 being a condensation product of methylaminothiazole and 3-bromo-5-chlorosalicylaldehyde exhibits no inhibition towards cancer cells under the experimental conditions (Table 6). Among these ligands, HL_3 exhibits maximum percentage inhibition as aminothiazole is sterically more demanding (R = R_1 = H). Therefore a dose–response curve of ligand HL_3 (Figure 7) compared to standard drugs was obtained with concentration ranging from 30 to 0.2 μg ml^{-1}. Complexes derived from ligand HL_1, i.e. $[Co(L_1)_2(H_2O)_2]$, $[Ni(L_1)_2(H_2O)_2]$ and $[Zn(L_1)_2]$, show a several-fold increase in activity as compared to the free ligand. One of the complexes, $[Ni(L_1)_2(H_2O)_2]$, exhibited promising activity, and therefore a dose–response curve of the complex (Figure 8) was obtained in a similar manner as discussed earlier. Other metal complexes exhibit moderate or no inhibition and none of the ligands and complexes was better than the standard used.

3.12 | Protein binding studies

Intermolecular interactions that occur due to various processes such as excited-state reactions, molecular rearrangements, energy transfer, ground-state complex formation and collision quenching can be easily studied using the fluorescence quenching mechanism.[33] The fluorescence spectra of metal complexes **1**–**4** in the presence of BSA have a strong emission band (λ_{em}) at 327 nm, which corresponds to tryptophan residues of BSA. It was expected that metal complexes would interact with the tryptophan residues of BSA. To investigate this, fluorescence quenching was studied taking a fixed concentration of BSA and varying concentrations of metal complexes (6.62–33.2 μM) to evaluate the binding constant of **1**–**4** with BSA. The results clearly show that keeping BSA concentration constant and increasing the concentration of metal complexes leads to a considerable decrease in the fluorescence intensity of BSA. This might be possible because of the complexation of BSA with metal complexes. A similar change in the intensity of BSA fluorescence after metal complexation has been reported in the literature.[34]

For metal complex **1**, the red shift observed was because of the increase in polarity of the microenvironment around the tryptophan residue after metal complexation. Probably, the loss of compact structure in the hydrophobic subdomain II where tryptophan-214 is placed caused this shift.[35] Similarly, on addition of nickel complex **2** and copper complex **3** in varying concentrations to BSA causes a red shift from 327 to 337 nm for **2**,

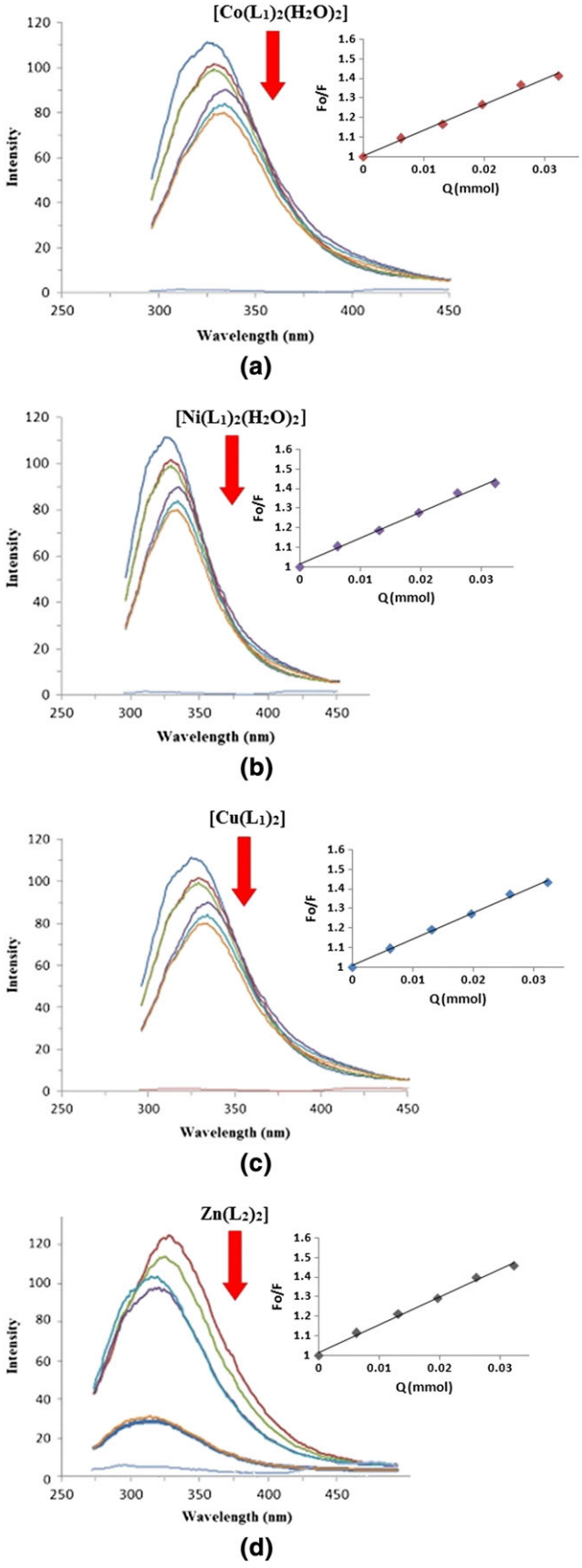

FIGURE 9 Fluorescence quenching spectra and Stern–Volmer plots of BSA for various concentrations of complexes: (a) **1**, (b) **2**, (c) **3**, (d) **4**; [BSA] = 15 μM; [**1**–**4**] = 6.62–32.2 μM

while for **3** a shift from 327 to 334 nm was observed. However, the addition of zinc complex **4** to BSA in varying amounts caused a blue shift of 8 nm. Some studies in the literature reveal that interactions between molecules, i.e. PAAB, vitamin B_{12} and colchicines, with BSA cause a blue shift of around 5–8.5 nm in the emission spectra.[36] Possibly this blue shift is observed because of an increase in hydrophobicity and decrease in polarity around the tryptophan residue.

To investigate further the fluorescence data were analysed using the Stern–Volmer equation: $F_0/F = 1 + K_{sv}[Q]$, where K_{sv} is the Stern–Volmer quenching constant, F_0 is the fluorescence intensity of BSA in the absence of quencher molecule, F is the fluorescence intensity of BSA in the presence of quencher molecule and [Q] is the concentration of the quencher metal complex. Figure 9 displays the Stern–Volmer plots of metal complexes **1**–**4** with BSA. Bimolecular quenching rate constant (K_q) was calculated using the following relation:

$$\frac{F_0}{F} = 1 + K_{sv}[Q] = 1 + K_q\tau_0[Q]$$

where K_q is the bimolecular quenching rate constant, τ_0 is the lifetime of BSA in the absence of quencher and K_{sv} is the Stern–Volmer constant. The calculated values of K_{sv} and K_q for metal complexes **1**–**4** are given in Table 7. The number of binding sites was also calculated using the fluorescence quenching data with the following equation:

$$\log\frac{F_0 - F}{F} = \log K_b + n\log[Q]$$

where K_b and n are the binding constant and number of binding sites for metal complexes **1**–**4**. The value of K_b indicates that Cu and Zn complexes bind strongly to BSA in comparison to Co and Ni complexes. For Cu and Zn complexes, the value of n calculated is near to 1, indicating the high affinity of binding sites of albumins. The binding constant and number of binding sites are given in Table 8.

TABLE 7 Stern–Volmer constants and bimolecular quenching rate constants for metal complexes **1**–**4**

Complex	K_{sv} (mol^{-1})	K_q (mol^{-1} s^{-1})	R^2
1	3.564×10^3	3.621×10^{12}	0.976
2	3.367×10^3	3.435×10^{12}	0.954
3	3.601×10^3	3.298×10^{12}	0.991
4	3.532×10^3	3.387×10^{12}	0.993

TABLE 8 Binding constants and number of binding sites for metal complexes **1**–**4**

Complex	K_b	n	R^2
1	2.99×10^3	0.987	0.945
2	2.86×10^3	0.991	0.923
3	3.13×10^3	0.999	0.931
4	6.41×10^3	1.04	0.967

4 | CONCLUSIONS

Schiff bases obtained by the condensation of aminothiazole and substituted salicylaldehyde are confirmed using spectral techniques. The synthesized Schiff bases act as uni-negative bidentate ligands and coordinate through azomethine nitrogen and deprotonated phenolic oxygen. Based on the results obtained through various spectroscopic techniques, Co(II) and Ni(II) complexes show octahedral geometry, while Cu(II) and Zn(II) complexes show four-coordinated geometry. The presence of coordinated water molecules in metal complexes was confirmed from IR and TGA data. All the synthesized compounds have been investigated for *in vitro* antibacterial activity and cytotoxicity against HepG2 (liver hepatocellular) cell line. Some of the complexes showed enhanced activity as compared to the parent ligand.

ACKNOWLEDGEMENTS

One of the authors (A.P.) is grateful to CSIR (Council of Science and Industrial Research) New Delhi for providing JRF fellowship wide letter no. 09/752/(0045)/2012-EMR-1. The authors are also grateful to TCG Life Sciences (Biology Section), Kolkata for antibacterial and cytotoxic studies of compounds reported herein.

REFERENCES

[1] R. Jain, A. P. Mishra, *Jordan J. Chem.* **2012**, *7*, 9.

[2] P. K. Sahu, P. K. Sahu, D. Thavaselvam, A. M. Alafeefy, D. D. Agarwal, *Med. Chem. Res.* **2015**, *24*, 725.

[3] P. Ali, J. Meshram, V. Tiwari, *Int. J. ChemTech Res.* **2010**, *2*, 956.

[4] N. Vukovic, S. Sukdolak, S. Solujic, T. Milosevic, *Arch. Pharm. Chem. Life Sci.* **2008**, *341*, 491.

[5] Y. Jiao, Q. Shenyi, H. Aixi, P. Junmei, Q. Zhi, *Chem. Res. Chin. Univ.* **2014**, *30*, 49.

[6] X. Zhou, L. Shao, Z. Jin, J. B. Liu, H. Dai, J. X. Fang, *Heteroatom Chem.* **2007**, *18*, 55.

[7] R. M. Mohareb, D. H. Fleita, O. K. Sakka, *Molecules* **2011**, *16*, 16.

[8] K. Rehse, T. Baselt, *Arch. Pharm. Chem. Life Sci.* **2008**, *341*, 645.

[9] P. Mondal, M. Banerjee, S. Jana, A. Bose, *J. Young Pharm.* **2010**, *2*, 169.

[10] J. Geng, M. Li, L. Wu, J. Ren, X. Qu, *J. Med. Chem.* **2012**, *55*, 9146.

[11] J. V. Metzger (Ed), *The Chemistry of Heterocyclic Compounds: Thiazole and Its Derivatives*, Vol. 34, Wiley, Chichester **1979**.

[12] H. D. Troutman, L. M. Long, *J. Am. Chem. Soc.* **2048**, *70*, 3436.

[13] B. E. Fink, D. S. Mortenson, S. R. Stauffer, Z. D. Aron, J. A. Katzenellenbogen, *Chem. Biol.* **1999**, *6*, 205.

[14] Z. H. Chohan, M. U. Hassan, K. M. Khan, C. T. Supuran, *J. Enz. Inhib. Med. Chem.* **2005**, *20*, 183.

[15] Z. H. Chohan, M. Praveen, *Appl. Organometal. Chem.* **2000**, *14*, 376.

[16] R. Malhotra, J. Mehta, K. Bala, A. K. Sharma, *Indian J. Chem.* **2008**, *47A*, 58.

[17] J. Devi, N. Batra, R. Malhotra, *Spectrochim. Acta A* **2012**, *97*, 397.

[18] R. Malhotra, J. Mehta, J. K. Puri, *Cent. Eur. J. Chem.* **2007**, *5*, 858.

[19] J. Devi, S. Kumari, R. Malhotra, *Phosphorus, Sulfur Silicon Relat. Elem.* **2012**, *187*, 587.

[20] I. Wiegand, K. Hilpert, R. E. W. Hancock, *Nat. Protoc.* **2008**, *3*, 163.

[21] M. J. Frisch, G. W. Trucks, H. B. Schlegel, G. E. Scuseria, M. A. Robb, J. R. Cheeseman, G. Scalmani, V. Barone, B. Mennucci, G. A. Petersson, H. Nakatsuji, M. Caricato, X. Li, H. P. Hratchian, A. F. Izmaylov, J. Bloino, G. Zheng, J. L. Sonnenberg, M. Hada, M. Ehara, K. Toyota, R. Fukuda, J. Hasegawa, M. Ishida, T. Nakajima, Y. Honda, O. Kitao, H. Nakai, T. Vreven, J. A. Montgomery Jr, J. E. Peralta, F. Ogliaro, M. Bearpark, J. J. Heyd, E. Brothers, K. N. Kudin, V. N. Staroverov, R. Kobayashi, J. Normand, K. Raghavachari, A. Rendell, J. C. Burant, S. S. Iyengar, J. Tomasi, M. Cossi, N. Rega, J. M. Millam, M. Klene, J. E. Knox, J. B. Cross, V. Bakken, C. Adamo, J. Jaramillo, R. Gomperts, R. E. Stratmann, O. Yazyev, A. J. Austin, R. Cammi, C. Pomelli, J. W. Ochterski, R. L. Martin, K. Morokuma, V. G. Zakrzewski, G. A. Voth, P. Salvador, J. J. Dannenberg, S. Dapprich, A. D. Daniels, O. Farkas, J. B. Foresman, J. V. Ortiz, J. Cioslowski, D. J. Fox, Gaussian 09, Gaussian Inc., Wallingford, CT, **2009**.

[22] M. A. D. Becke, *Phys. Rev. A* **1988**, *38*, 3098.

[23] C. Lee, W. Yang, R. G. Parr, *Phys. Rev. B* **1988**, *37*, 785.

[24] S. H. Vosko, L. Wilk, M. Nusair, *Can. J. Chem.* **1980**, *58*, 1200.

[25] W. J. Geary, *Coord. Chem. Rev.* **1971**, *7*, 81.

[26] P. Tyagi, S. Chandra, B. S. Saraswat, D. Sharma, *Spectrochim. Acta A* **2015**, *143*, 1.

[27] P. Tyagi, S. Chandra, B. S. Saraswat, *Spectrochim. Acta A* **2015**, *134*, 200.

[28] M. Tyagi, S. Chandra, P. Tyagi, *Spectrochim. Acta A* **2014**, *117*, 1.

[29] P. Tyagi, M. Tyagi, S. Agrawal, S. Chandra, H. Ojha, M. Pathak, *Spectrochim. Acta A* **2017**, *171*, 246.

[30] S. Chandra, S. Bargujar, R. Nirwal, N. Yadav, *Spectrochim. Acta A* **2013**, *106*, 91.

[31] A. B. P. Lever, *Inorganic Electronic Spectroscopy*, 2nd ed., Elsevier, Amsterdam **1984**.

[32] R. K. Ray, G. B. Kaufman, *Inorg. Chim. Acta* **1990**, *173*, 207.

[33] Y. J. Hu, Y. Liu, L. X. Zhang, *J. Mol. Struct.* **2005**, *750*, 174.

[34] S. Li, K. Huang, M. Zhong, J. Guo, W. Z. Wang, R. Zhu, *Spectrochim. Acta A* **2010**, *77*, 680.

[35] A. J. Sulkowska, *J. Mol. Struct.* **2002**, *614*, 227.

[36] Y. J. Hu, Y. Liu, L. X. Zhang, R. M. Zhao, S. S. Qu, *J. Mol. Struct.* **2002**, *750*, 174.

How to cite this article: Prakash A, Malhotra R. Co(II), Ni(II), Cu(II) and Zn(II) complexes of aminothiazole-derived Schiff base ligands: Synthesis, characterization, antibacterial and cytotoxicity evaluation, bovine serum albumin binding and density functional theory studies. *Appl Organometal Chem*. 2017;e4098. https://doi.org/10.1002/aoc.4098